
Kinematics of the Galaxy from OB Stars with Data from the Gaia DR2 Catalogue

V.V. Bobylev¹ and A.T. Bajkova

*Pulkovo Astronomical Observatory, Russian Academy of Sciences,
Pulkovskoe sh. 65, St. Petersburg, 196140 Russia*

Abstract—We have selected and analyzed a sample of OB stars with known line-of-sight velocities determined through ground-based observations and with trigonometric parallaxes and proper motions from the Gaia DR2 catalogue. Some of the stars in our sample have distance estimates made from calcium lines. A direct comparison with the trigonometric distance scale has shown that the calcium distance scale should be reduced by 13%. The following parameters of the Galactic rotation curve have been determined from 495 OB stars with relative parallax errors less than 30%: $(U, V, W)_{\odot} = (8.16, 11.19, 8.55) \pm (0.48, 0.56, 0.48)$ km s⁻¹, $\Omega_0 = 28.92 \pm 0.39$ km s⁻¹ kpc⁻¹, $\Omega'_0 = -4.087 \pm 0.083$ km s⁻¹ kpc⁻² and $\Omega''_0 = 0.703 \pm 0.067$ km s⁻¹ kpc⁻³, where the circular velocity of the local standard of rest is $V_0 = 231 \pm 5$ km s⁻¹ (for the adopted $R_0 = 8.0 \pm 0.15$ kpc). The parameters of the Galactic spiral density wave have been found from the series of radial, V_R , residual tangential, ΔV_{circ} , and vertical, W , velocities of OB stars by applying a periodogram analysis. The amplitudes of the radial, tangential, and vertical velocity perturbations are $f_R = 7.1 \pm 0.3$ km s⁻¹, $f_{\theta} = 6.5 \pm 0.4$ km s⁻¹, and $f_W = 4.8 \pm 0.8$ km s⁻¹, respectively; the perturbation wavelengths are $\lambda_R = 3.3 \pm 0.1$ kpc, $\lambda_{\theta} = 2.3 \pm 0.2$ kpc, and $\lambda_W = 2.6 \pm 0.5$ kpc; and the Sun's radial phase in the spiral density wave is $(\chi_{\odot})_R = -135 \pm 5^{\circ}$, $(\chi_{\odot})_{\theta} = -123 \pm 8^{\circ}$, and $(\chi_{\odot})_W = -132 \pm 21^{\circ}$ for the adopted four-armed spiral pattern.

DOI: 10.1134/S1063773718110026

INTRODUCTION

Stars of spectral types O and B are extremely young, are distributed over the entire Galactic disk, and are located virtually where they were born. Such stars are members of active star-forming regions, stellar associations, and open star clusters (OSCs). All of this makes them very important objects in studying the kinematics and dynamics of the Galaxy as well as its spiral structure.

Until recently, it had been possible to use only the estimates based on the analysis of photometric and spectroscopic data as the distances to OB stars, because, for example, the Hipparcos catalogue (1997) contains only ~ 250 OB5 stars with a parallax error $< 15\%$ (Maiz-Apellániz 2001). The mean error of the photometric distance estimate is $\sim 20\%$. The distances to OB stars inferred from interstellar calcium lines, whose mean error is estimated to be 15%, proved to be good (Megier et al. 2005, 2009; Galazutdinov et al.

¹e-mail: vbobylev@gaoran.ru

2015). Important results were obtained by various authors using the group distances to OB stars when analyzing young OB associations and OSCs, whose mean error is estimated to be 15–20% (Blaha and Humphreys 1989; Zabolotskikh et al. 2002; Mel’nik and Dambis 2009, 2017). Reliable trigonometric parallax estimates for OB stars have been obtained only recently.

For example, the Gaia data processing results after the first year of its in-orbit operation were published in September 2016 (Prusti et al. 2016; Brown et al. 2016). Its catalogue contains the trigonometric parallaxes and proper motions of ~ 2 billion stars. The mean parallax error is about 0.3 mas. For some of the stars (TGAS, Tycho–Gaia Astrometric Solution) their proper motions were determined with a mean epoch difference of about 24 years with a mean error of about 0.06 mas yr^{-1} for the stars common to the Hipparcos catalogue (1997) and $\sim \text{mas yr}^{-1}$ for the remaining stars (Brown et al. 2016). Using these data, various authors performed a number of important studies devoted to the kinematics of stars from the solar neighborhood (Bovy 2017; Hunt et al. 2017; Bobylev and Bajkova 2017; Vityazev et al. 2017).

The Gaia second data release, Gaia DR2, was published in April 2018 (Brown et al. 2018; Lindegren et al. 2018), while its third data release is planned to be issued in mid-2020. The Gaia DR2 catalogue contains the trigonometric parallaxes and proper motions of ~ 1.7 billion stars. The derivation of their values is based on the orbital observations performed for 22 months. The mean errors of the trigonometric parallax and both proper motion components in this catalogue depend on magnitude. For example, the parallax errors lie in the range 0.02–0.04 mas for bright stars ($G < 15^m$) and are 0.7 mas for faint stars ($G = 20^m$).

It is important to note that the spatial motions of ~ 7 million stars for which not only their highly accurate parallaxes and proper motions, but also their line-of-sight velocities were measured with mean errors less than 1.8 km s^{-1} can be thoroughly analyzed on the basis of Gaia DR2. However, there are some classes of objects for which the Gaia DR2 catalogue has no line-of-sight velocity estimates. These include, for example, spectroscopic binary OB stars or Cepheids for which determining the line-of-sight velocities requires special long-term observations.

The goal of this paper is to improve the Galactic rotation parameters and the parameters of the Galactic spiral density wave based on OB stars using their highly accurate trigonometric parallaxes and proper motions taken from the Gaia DR2 catalogue with the involvement of their line-of-sight velocities measured previously by ground-based methods.

METHODS

We know three stellar velocity components from observations: the line-of-sight velocity V_r and the two tangential velocity components $V_l = 4.74r\mu_l \cos b$ and $V_b = 4.74r\mu_b$ along the Galactic longitude l and latitude b , respectively, expressed in km s^{-1} . Here, the coefficient 4.74 is the ratio of the number of kilometers in an astronomical unit to the number of seconds in a tropical year, and r is the stellar heliocentric distance in kpc. The proper motion components $\mu_l \cos b$ and μ_b are expressed in mas yr^{-1} . The velocities U, V, W directed along the rectangular Galactic coordinate axes are calculated via the components V_r, V_l, V_b :

$$\begin{aligned} U &= V_r \cos l \cos b - V_l \sin l - V_b \cos l \sin b, \\ V &= V_r \sin l \cos b + V_l \cos l - V_b \sin l \sin b, \\ W &= V_r \sin b + V_b \cos b, \end{aligned} \tag{1}$$

where the velocity U is directed from the Sun toward the Galactic center, V is in the direction of Galactic rotation, and W is directed to the north Galactic pole. We can find two velocities, V_R directed radially away from the Galactic center and the circular velocity V_{circ} orthogonal to it pointing in the direction of Galactic rotation, from the following equations:

$$\begin{aligned} V_{circ} &= U \sin \theta + (V_0 + V) \cos \theta, \\ V_R &= -U \cos \theta + (V_0 + V) \sin \theta, \end{aligned} \quad (2)$$

where the position angle θ obeys the relation $\tan \theta = y/(R_0 - x)$, and x, y, z are the rectangular heliocentric coordinates of the star (the velocities U, V, W are directed along the corresponding x, y, z axes).

To determine the parameters of the Galactic rotation curve, we use the equations derived from Bottlinger's formulas, in which the angular velocity Ω is expanded into a series to terms of the second order of smallness in r/R_0 :

$$\begin{aligned} V_r &= -U_\odot \cos b \cos l - V_\odot \cos b \sin l - W_\odot \sin b \\ &+ R_0(R - R_0) \sin l \cos b \Omega'_0 \\ &+ R_0(R - R_0)^2 \sin l \cos b \Omega''_0/2, \\ &+ R_0(R - R_0)^3 \sin l \cos b \Omega'''_0/6, \end{aligned} \quad (3)$$

$$\begin{aligned} V_l &= U_\odot \sin l - V_\odot \cos l - r \Omega_0 \cos b \\ &+ (R - R_0)(R_0 \cos l - r \cos b) \Omega'_0 \\ &+ (R - R_0)^2 (R_0 \cos l - r \cos b) \Omega''_0/2, \\ &+ (R - R_0)^3 (R_0 \cos l - r \cos b) \Omega'''_0/6, \end{aligned} \quad (4)$$

$$\begin{aligned} V_b &= U_\odot \cos l \sin b + V_\odot \sin l \sin b - W_\odot \cos b \\ &- R_0(R - R_0) \sin l \sin b \Omega'_0 \\ &- R_0(R - R_0)^2 \sin l \sin b \Omega''_0/2, \\ &- R_0(R - R_0)^3 \sin l \sin b \Omega'''_0/6, \end{aligned} \quad (5)$$

where R is the distance from the star to the Galactic rotation axis:

$$R^2 = r^2 \cos^2 b - 2R_0 r \cos b \cos l + R_0^2. \quad (6)$$

The quantity Ω_0 is the angular velocity of Galactic rotation at the solar distance R_0 , the parameters Ω'_0 , Ω''_0 and Ω'''_0 are the first, second, and third derivatives of the angular velocity, respectively, and $V_0 = |R_0 \Omega_0|$.

A number of studies devoted to determining the mean distance from the Sun to the Galactic center using its individual determinations in the last decade by independent methods have been performed by now. For example, $R_0 = 8.0 \pm 0.2$ kpc (Vallée 2017a), $R_0 = 8.4 \pm 0.4$ kpc (de Grijs and Bono 2017), or $R_0 = 8.0 \pm 0.15$ kpc (Camarillo et al. 2018). Based on these reviews, in this paper we adopted $R_0 = 8.0 \pm 0.15$ kpc.

The influence of the spiral density wave in the radial (V_R) and residual tangential (ΔV_{circ}) velocities is periodic with an amplitude of ~ 10 km s⁻¹. According to the linear theory of density waves (Lin and Shu 1964), it is described by the following relations:

$$\begin{aligned} V_R &= -f_R \cos \chi, \\ \Delta V_{circ} &= f_\theta \sin \chi, \end{aligned} \quad (7)$$

where

$$\chi = m[\cot(i) \ln(R/R_0) - \theta] + \chi_\odot \quad (8)$$

is the phase of the spiral density wave (m is the number of spiral arms, i is the pitch angle of the spiral pattern, and χ_\odot is the Sun's radial phase in the spiral density wave); f_R and f_θ are the amplitudes of the radial and tangential velocity perturbations, which are assumed to be positive. As an analysis of the present day highly accurate data showed, the periodicities associated with the spiral density wave also manifest themselves in the vertical velocities W (Bobylev and Bajkova 2015; Rastorguev et al. 2017).

We apply a spectral analysis to study the periodicities in the velocities V_R , ΔV_{circ} and W . The wavelength λ (the distance between adjacent spiral arm segments measured along the radial direction) is calculated from the relation

$$\frac{2\pi R_0}{\lambda} = m \cot(i). \quad (9)$$

Let there be a series of measured velocities V_{R_n} (these can be the radial (V_R), tangential (ΔV_{circ}), and vertical (W) velocities), $n = 1, \dots, N$, where N is the number of objects. The objective of our spectral analysis is to extract a periodicity from the data series in accordance with the adopted model describing a spiral density wave with parameters f , λ (or i) and χ_\odot .

Having taken into account the logarithmic behavior of the spiral density wave and the position angles of the objects θ_n , our spectral (periodogram) analysis of the series of velocity perturbations is reduced to calculating the square of the amplitude (power spectrum) of the standard Fourier transform (Bajkova and Bobylev 2012):

$$\bar{V}_{\lambda_k} = \frac{1}{N} \sum_{n=1}^N V'_n(R'_n) \exp\left(-j \frac{2\pi R'_n}{\lambda_k}\right), \quad (10)$$

where \bar{V}_{λ_k} is the k th harmonic of the Fourier transform with wavelength $\lambda_k = D/k$, D is the period of the series being analyzed,

$$\begin{aligned} R'_n &= R_0 \ln(R_n/R_0), \\ V'_n(R'_n) &= V_n(R'_n) \times \exp(jm\theta_n). \end{aligned} \quad (11)$$

The sought-for wavelength λ corresponds to the peak value of the power spectrum S_{peak} . The pitch angle of the spiral density wave is derived from Eq. (9). We determine the perturbation amplitude and phase by fitting the harmonic with the wavelength found to the observational data. The following relation can also be used to estimate the perturbation amplitude:

$$f_R(f_\theta, f_W) = 2 \times \sqrt{S_{peak}}. \quad (12)$$

Thus, our approach consists of two steps: (i) the construction of a smooth Galactic rotation curve and (ii) a spectral analysis of the radial (V_R), residual tangential (ΔV_{circ}), and vertical (W) velocities. Such a method was applied by Bobylev and Bajkova (2012, 2013, 2015, 2017) to study the kinematics of young Galactic objects.

DATA

In this paper we use a sample of 554 OB stars. It includes:

- (i) 266 single OB stars whose distances were determined previously (Megier et al. 2005, 2009; Galazutdinov et al. 2015) from interstellar Ca II lines;

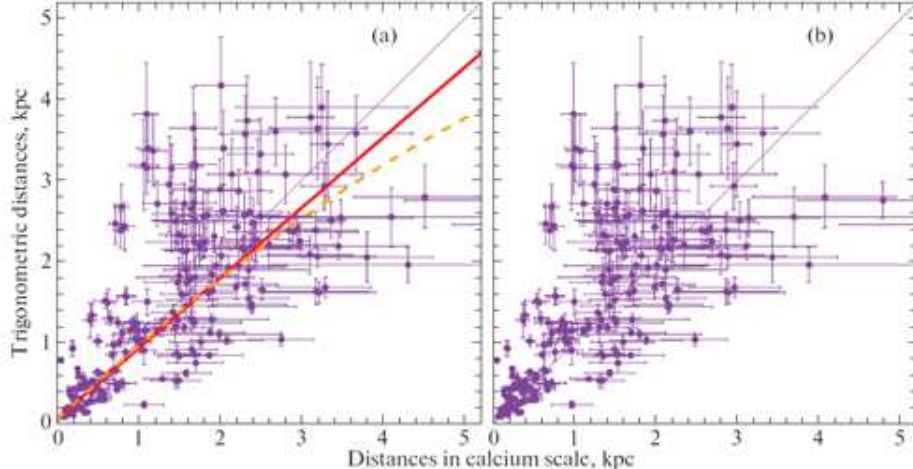


Figure 1: (Color online) (a) Distances calculated from the Gaia DR2 trigonometric parallaxes versus distances to the stars inferred from interstellar calcium lines; (b) the same, but the calcium distance scale was reduced by 10%. The thin line corresponds to the expected dependence with a correlation coefficient equal to one, the thick line indicates the linear dependence with parameters (14), and the dashed line indicates the quadratic dependence with parameters (15).

(ii) 189 spectroscopic binary OB stars from Bobylev and Bajkova (2013, 2015); this list includes binaries with spectral types of the primary component no later than B2.5 and various supergiants with luminosity classes Ia and Iab;

(iii) 99 single OB stars with spectral types no later than B2.5 that we selected previously (Bobylev and Bajkova 2013, 2015) based on the criterion of a small (less than 10%) relative trigonometric parallax error in the Hipparcos catalogue (1997).

For all the listed OB stars of our sample we took the trigonometric parallaxes and proper motion components from the Gaia DR2 catalogue (Brown et al. 2018).

We collected the line-of-sight velocities from published sources. This is particularly important for spectroscopic binary OB stars, because reliable systemic line-of-sight velocities for such binaries are determined only through long-term spectroscopic observations and subsequent analysis of their orbital motion. The continuously updatable SB9 bibliographic database (Pourbaix et al. 2004) is a very important source of information about the results of an orbital analysis of spectroscopic binaries.

RESULTS AND DISCUSSION

Comparison with the Calcium Distance Scale

We have a homogeneous set of OB stars whose distances were determined from interstellar calcium lines at our disposal. This distance scale is of interest for kinematic studies. Therefore, it is important to compare these distances with the trigonometric ones.

In Fig. 1 the distances to the OB stars calculated from the Gaia DR2 trigonometric parallaxes are plotted against their distances inferred from interstellar calcium lines. It can be seen from Fig. 1a that the calcium distance scale is slightly longer than the trigonometric

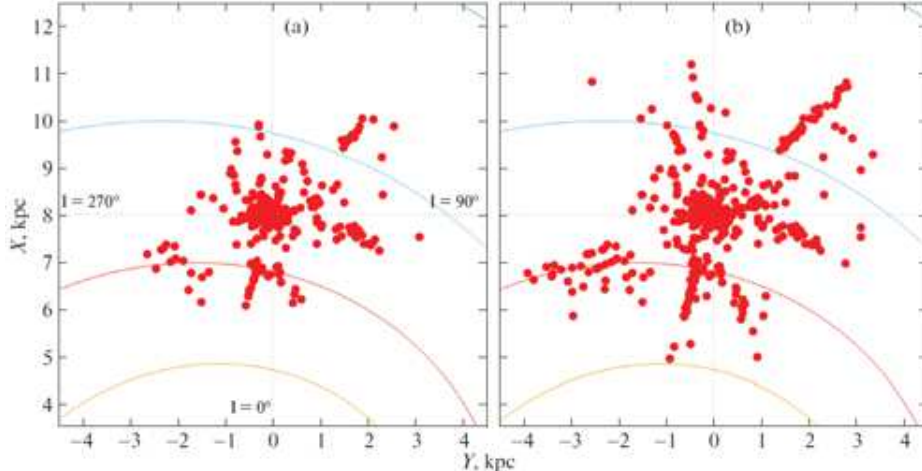


Figure 2: (Color online) (a) Projection of the OB stars with relative trigonometric parallax errors less than 10% onto the Galactic XY plane; (b) the same, but with relative trigonometric parallax errors less than 30%. Segments of the four-armed spiral pattern with a pitch angle of -13° constructed as prescribed by Bobylev and Bajkova (2014) are shown.

one. However, the effect is tangible only at distances greater than 2 kpc. We decided to analytically check the difference between the distance scales based on the following relation:

$$d_{trig} = a + b \cdot d_{CaII} + c \cdot d_{CaII}^2. \quad (13)$$

A weight inversely proportional to the square of the errors, $p = 1/(\sigma_{d_{trig}}^2 + \sigma_{d_{CaII}}^2)$, was assigned to each conditional equation (13). As a result, we obtained the following solution of the system of conditional equations (13) by the least-squares method (LSM) based on a sample of 228 OB stars with two unknowns:

$$\begin{aligned} a &= 0.05 \pm 0.02 \text{ kpc}, \\ b &= 0.87 \pm 0.05, \end{aligned} \quad (14)$$

and with three unknowns:

$$\begin{aligned} a &= 0.04 \pm 0.02 \text{ kpc}, \\ b &= 0.95 \pm 0.11, \\ c &= -0.042 \pm 0.048 \text{ kpc}^{-1}. \end{aligned} \quad (15)$$

Both dependences found, the linear (14) and quadratic (15) ones, are presented in Fig. 1a.

The approach based on the solution (14) is simplest. Here the parameter b acts as a scale factor. We proceed from the assumption that the distance scale specified by the trigonometric parallaxes from the Gaia DR2 catalogue is most accurate. The value of $b = 0.87$ suggests that all distances to the OB stars with the calcium distance scale should be reduced by 13%. In the approach based on the solution (15) we have a variable scale factor. For example, at a distance of 3 kpc the scale factor is 0.82.

Figure 1b provides the distances to the OB stars where the calcium distance scale was reduced by 10%. We see that such a reduction of the calcium distance scale makes the distribution of points on the diagram more symmetric relative to the diagonal, although it does not rule out completely the tail at very large (>4 kpc) distances.

Table 1: The Galactic rotation parameters found from OB stars with their proper motions and trigonometric parallaxes from the Gaia DR2 catalogue for various constraints on the relative parallax error. The results obtained by excluding the Gould Belt stars are given at the bottom

Parameters	$\sigma_\pi/\pi < 10\%$	$\sigma_\pi/\pi < 20\%$	$\sigma_\pi/\pi < 30\%$	$\sigma_\pi/\pi < 100\%$
U_\odot , km s ⁻¹	8.67 ± 0.57	8.52 ± 0.51	8.44 ± 0.52	8.54 ± 0.55
V_\odot , km s ⁻¹	13.28 ± 0.65	11.70 ± 0.59	11.59 ± 0.60	11.36 ± 0.65
Ω_0 , km s ⁻¹ kpc ⁻¹	30.21 ± 0.67	28.45 ± 0.47	28.78 ± 0.45	28.85 ± 0.43
Ω'_0 , km s ⁻¹ kpc ⁻²	-4.36 ± 0.14	-4.098 ± 0.098	-4.073 ± 0.091	-4.060 ± 0.087
Ω''_0 , km s ⁻¹ kpc ⁻³	1.05 ± 0.15	0.746 ± 0.076	0.723 ± 0.073	0.710 ± 0.081
Ω'''_0 , km s ⁻¹ kpc ⁻⁴	—	—	—	-0.025 ± 0.021
σ_0 , km s ⁻¹	9.68	10.85	11.33	12.26
N_\star	306	467	495	511
A , km s ⁻¹ kpc ⁻¹	17.43 ± 0.54	16.39 ± 0.38	16.29 ± 0.36	16.24 ± 0.35
B , km s ⁻¹ kpc ⁻¹	-12.79 ± 0.86	-12.06 ± 0.61	-12.49 ± 0.58	-12.61 ± 0.56
V_0 , km s ⁻¹	242 ± 6	228 ± 6	230 ± 6	231 ± 6
U_\odot , km s ⁻¹	6.72 ± 0.97	6.79 ± 0.71	6.44 ± 0.73	6.84 ± 0.78
V_\odot , km s ⁻¹	10.36 ± 1.29	8.78 ± 0.94	8.96 ± 0.95	8.91 ± 1.05
Ω_0 , km s ⁻¹ kpc ⁻¹	28.92 ± 0.81	28.45 ± 0.51	28.69 ± 0.50	29.12 ± 0.50
Ω'_0 , km s ⁻¹ kpc ⁻²	-4.15 ± 0.16	-4.075 ± 0.102	-4.042 ± 0.101	-4.129 ± 0.099
Ω''_0 , km s ⁻¹ kpc ⁻³	0.82 ± 0.20	0.612 ± 0.090	0.590 ± 0.088	0.609 ± 0.103
Ω'''_0 , km s ⁻¹ kpc ⁻⁴	—	—	—	-0.006 ± 0.027
σ_0 , km s ⁻¹	11.56	11.70	12.58	13.86
N_\star	154	285	310	325
A , km s ⁻¹ kpc ⁻¹	16.58 ± 0.65	16.30 ± 0.41	16.17 ± 0.40	16.52 ± 0.40
B , km s ⁻¹ kpc ⁻¹	-12.34 ± 1.04	-12.14 ± 0.65	-12.52 ± 0.65	-12.60 ± 0.63

Based on the kinematic method, Bobylev and Bajkova (2011) showed that the calcium distance scale is extended approximately by 20%. This conclusion was reached for part of the sample of OB stars with distances exceeding 0.8 kpc considered in this paper. It is important that the conclusion about the necessity of reducing the calcium distance scale was corroborated by an independent method. This allows the results of our kinematic analysis of OB stars obtained in this paper to be compared with those obtained by us previously with a reduction of the calcium distance scale without taking any additional measures.

Apart from the scale factor b (see Eq. (13)), the possible systematic shift $\Delta\pi$ in the stellar parallaxes from the Gaia DR2 catalogue with respect to an inertial frame of reference of great interest. However, a highly accurate calibration sample of stars that we do not have in this paper is needed for its determination.

But Lindegren et al. (2018) have already pointed out the existence of such a shift with $\Delta\pi = -0.029$ mas. At present, there are several reliable distance scales a comparison with which allows, in the opinion of their authors, the systematics in the Gaia trigonometric parallaxes to be controlled. For example, by comparing the parallaxes of 89 stars from the Gaia DR2 catalogue and calibration eclipsing binary stars, Stassun and Torres (2018) found a shift between the systems $\Delta\pi = -0.082 \pm 0.033$ mas. Such a value also finds a confirmation in the works of our authors. In particular, $\Delta\pi = -0.046 \pm 0.013$ mas (Riess et al. 2018) and $\Delta\pi = -0.083 \pm 0.002$ mas (Zinn et al. 2018) when analyzing Cepheids and astroseismological

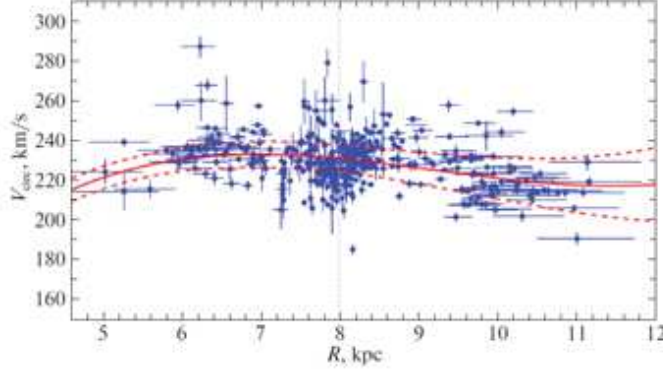


Figure 3: (Color online) Circular velocities of OB stars with relative trigonometric parallax errors less than 20%, the Galactic rotation curve constructed according to the solution (19) with the boundaries of 1σ confidence intervals is presented, the vertical dotted line marks the Sun’s position.

data, respectively.

We solved the system of equations (13) by the LSM based on a sample of 228 OB stars, where the trigonometric distances were corrected for the Lutz-Kelker bias. The corrections for this bias were calculated using Eq. (28) from Rastorguev et al. (2017), where a flat spatial distribution of stars is assumed. As a result, we obtained the following solution with two unknowns:

$$\begin{aligned} a &= 0.05 \pm 0.02 \text{ kpc}, \\ b &= 0.91 \pm 0.05, \end{aligned} \quad (16)$$

and with three unknowns:

$$\begin{aligned} a &= 0.03 \pm 0.02 \text{ kpc}, \\ b &= 0.99 \pm 0.11, \\ c &= -0.040 \pm 0.049 \text{ kpc}^{-1}. \end{aligned} \quad (17)$$

About 90% of the OB stars in our list have small relative trigonometric parallax errors, less than 20%. Therefore, the parameters found in the solutions (14), (16) and the solutions (15), (17) differ insignificantly.

Galactic Rotation Curve

The system of conditional equations (3)–(4) or (3)–(5) is solved by the LSM with weights of the form $w_r = S_0/\sqrt{S_0^2 + \sigma_{V_r}^2}$, $w_l = S_0/\sqrt{S_0^2 + \sigma_{V_l}^2}$ and $w_b = S_0/\sqrt{S_0^2 + \sigma_{V_b}^2}$, where S_0 is the “cosmic” dispersion, σ_{V_r} , σ_{V_l} , σ_{V_b} are the errors in the corresponding observed velocities. S_0 is comparable to the rms residual σ_0 (the error per unit weight) when solving the conditional equations (3)–(5). In this paper we adopted $S_0 = 10 \text{ km s}^{-1}$. For the preliminary exclusion of runaway stars we use only one constraint on the vertical velocity, $|W| < 40 \text{ km s}^{-1}$. The solutions are sought in two iterations with the elimination of large residuals according to the 3σ criterion.

Figure 2 shows the distributions of our sample OB stars in projection onto the Galactic XY plane for various constraints on the parallax errors. As can be seen from Fig. 2a, at a parallax error less than 10% the radius of the solar neighborhood is about 3 kpc. In this case, however, the Gould Belt and Local Arm stars constitute the bulk, while the nearest spiral

arm segments are barely distinguishable. Our study of the distributions of OB stars with various constraints on the parallax errors showed that to determine the Galactic rotation and spiral structure parameters, it is best to produce a sample with parallax errors 20–30% (Fig. 2b).

Table 1 gives the Galactic rotation parameters found from OB stars with various constraints on the relative parallax error. These parameters were derived when simultaneously solving only two equations, (3) and (4), with a different number of unknowns by the LSM. This approach to solving such a system of equations is commonly used in analyzing objects far from the Sun, because in this case the contribution of Eq. (5) is negligible due to the closeness of $\sin b$ typical for all our sample stars to zero. The peculiar solar velocity W was taken to be $W = 7 \text{ km s}^{-1}$. The results obtained from our sample with parallax errors less than 100% are given in the last column of the table. In this case the equations contained six unknowns to be determined using the third derivative in the expansion of the angular velocity of Galactic rotation. The number of OB stars used is denoted by N_* in the table.

Many authors use the Oort parameters to characterize the Galactic rotation. In particular, these include the Oort constants A and B that can be found from the following expressions:

$$A = -0.5\Omega'_0 R_0, \quad B = -\Omega_0 + A. \quad (18)$$

It can be seen from the top part of the table that the influence of the Gould Belt manifests itself in the sample of OB stars with parallax errors less than 10%. Compared to the results from other columns, the velocities V_\odot , Ω_0 and V_0 are large here. On the other hand, there are no significant differences between the parameters derived with the constraints on parallax errors less than 30% and less than 100%. The growth of the error σ_0 with increasing sample radius (increasing parallax error) is noticeable due to the influence of the proper motion and parallax errors, because the contribution of the line-of-sight velocity errors does not depend on the distance.

The results obtained by excluding the Gould Belt stars are given in the bottom part of the table. For this purpose, we rejected the stars located at distances less than 0.5 kpc. The exclusion of such stars affected mainly the results in the first column of the table. All of the parameters from the bottom part of the first column now hardly differ from those in other columns. Only the velocity V_\odot changed for all the results in the bottom part of the table. The differences in the remaining parameters are insignificant; the random errors increased due to a considerable number of stars.

Note the solutions obtained with six unknowns. As can be seen from the last column of the table, the third derivative of the angular velocity Ω_0''' turns out to be small. However, when the rotation curve is constructed from these data, the boundaries of the confidence intervals grow very dramatically toward the edge of the region under consideration due to the errors in Ω_0''' . Therefore, below we use the solutions obtained with the expansion of Ω_0 only to the second derivative.

It is pertinent to estimate the distance r at which the contributions of the random line-of-sight velocity errors σ_{V_r} and the proper motion errors σ_μ become equal. For this purpose, we use the relation $\sigma_{V_r} = 4.74\sigma_\mu r$. Then, for example, for $\sigma_{V_r} = 2 \text{ km s}^{-1}$ and $\sigma_\mu = 0.1 \text{ mas}$ we obtain $r = 4.2 \text{ kpc}$, i.e., farther than 4.5–5 kpc the errors of the Gaia DR2 proper motions dominate in the space velocities of the OB stars. But the main conclusion here is that in the solar neighborhood with a radius less than 4.5–5 kpc the random errors in the space velocities U , V , and W of the OB stars are small (usually less than 5–6 km s^{-1}), which is very useful, for example, for revealing runaway stars in this neighborhood.

Next, we simultaneously solve the system of three conditional equations (3)–(5). Based on a sample of 495 OB stars with relative trigonometric parallax errors less than 30%, we found the following kinematic parameters:

$$\begin{aligned}
(U_{\odot}, V_{\odot}, W_{\odot}) &= (8.16, 11.19, 8.55) \pm (0.48, 0.56, 0.48) \text{ km s}^{-1}, \\
\Omega_0 &= 28.92 \pm 0.39 \text{ km s}^{-1} \text{ kpc}^{-1}, \\
\Omega'_0 &= -4.087 \pm 0.083 \text{ km s}^{-1} \text{ kpc}^{-2}, \\
\Omega''_0 &= 0.703 \pm 0.067 \text{ km s}^{-1} \text{ kpc}^{-3}.
\end{aligned} \tag{19}$$

In this solution the error per unit weight is $\sigma_0 = 10.6 \text{ km s}^{-1}$, the Oort constants are $A = -16.35 \pm 0.33 \text{ km s}^{-1} \text{ kpc}^{-1}$ and $B = 12.58 \pm 0.51 \text{ km s}^{-1} \text{ kpc}^{-1}$, and the circular velocity of the local standard of rest is $V_0 = 231 \pm 5 \text{ km s}^{-1}$ for the distance $R_0 = 8.0 \pm 0.15 \text{ kpc}$ adopted in this paper.

Having analyzed the proper motions and parallaxes for a local sample of 304 267 main-sequence stars from the Gaia DR1 catalogue, Bovy (2017) obtained the following Oort parameters: $A = 15.3 \pm 0.5 \text{ km s}^{-1} \text{ kpc}^{-1}$ and $B = -11.9 \pm 0.4 \text{ km s}^{-1} \text{ kpc}^{-1}$, based on which he estimated the angular velocity of Galactic rotation to be $\Omega_0 = 27.1 \pm 0.5 \text{ km s}^{-1} \text{ kpc}^{-1}$ and the corresponding linear velocity to be $V_0 = 219 \pm 4 \text{ km s}^{-1}$. Since we used considerably younger stars in the solution (19), we obtained larger Ω_0 and V_0 . A different thing attracts our attention: we have three orders of magnitude fewer stars, but obtain identical and, in several cases, smaller errors in the parameters being determined.

It is interesting to compare the parameters (19) with the estimates by Rastorguev et al. (2017) from 130 masers with measured VLBI trigonometric parallaxes, where, in particular, the two solar velocity components are $(U_{\odot}, V_{\odot}) = (11.40, 17.23) \pm (1.33, 1.09) \text{ km s}^{-1}$ and the parameters of the Galactic rotation curve are $\Omega_0 = 28.93 \pm 0.53 \text{ km s}^{-1} \text{ kpc}^{-1}$, $\Omega'_0 = -3.96 \pm 0.07 \text{ km s}^{-1} \text{ kpc}^{-2}$ and $\Omega''_0 = 0.87 \pm 0.03 \text{ km s}^{-1} \text{ kpc}^{-3}$, $V_0 = 243 \pm 10 \text{ km s}^{-1}$ (for the value of $R_0 = 8.40 \pm 0.12 \text{ kpc}$ found). We can see that here there is excellent agreement in Ω_0 , Ω'_0 and Ω''_0 .

Figure 3 provides the circular velocities of OB stars with relative trigonometric parallax errors less than 20%; the Galactic rotation curve constructed according to the solution (19) is presented. We see that the random errors of the circular velocities for most stars are very small. At the same time, there are a number of OB stars whose velocities deviate noticeably from the smooth rotation curve (see also Fig. 5), i.e., they are candidates for runaway stars.

Parameters of the Spiral Density Wave

For our spectral analysis we used 462 OB stars with relative trigonometric parallax errors less than 20%. The residual circular velocities ΔV_{circ} were calculated from the deviation from the Galactic rotation curve (19). In this sense the velocities V_R and W are not residual, because they are virtually independent of the Galactic rotation curve.

Based on the series of radial, V_R , residual tangential, ΔV_{circ} , and vertical, W , velocities of this sample, we found the parameters of the Galactic spiral density wave with the application of a periodogram analysis. The amplitudes of the radial, tangential, and vertical velocity perturbations are $f_R = 7.1 \pm 0.3 \text{ km s}^{-1}$, $f_{\theta} = 6.5 \pm 0.4 \text{ km s}^{-1}$, $f_W = 4.8 \pm 0.8 \text{ km s}^{-1}$, respectively; the perturbation wavelengths are $\lambda_R = 3.3 \pm 0.1 \text{ kpc}$, $\lambda_{\theta} = 2.3 \pm 0.2 \text{ kpc}$ and $\lambda_W = 2.6 \pm 0.5 \text{ kpc}$ for the adopted four-armed spiral pattern ($m = 4$).

Figure 4 provides the power spectra of the radial, residual tangential, and vertical velocities for our sample of OB stars. Good agreement in the positions of the maxima, i.e.,

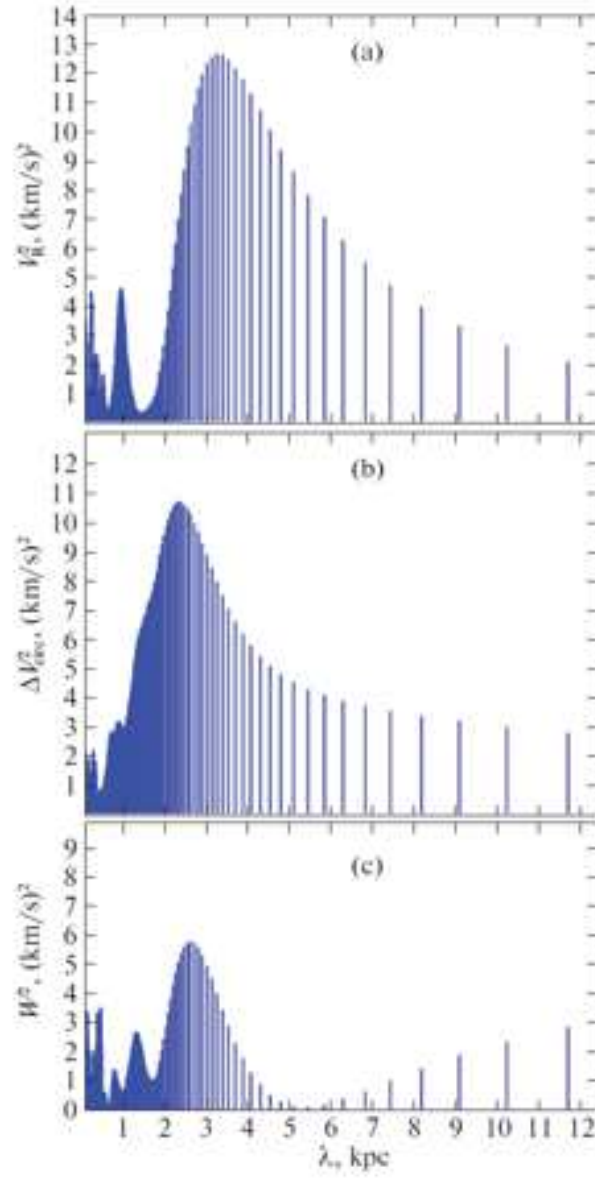


Figure 4: (Color online) Power spectra for the radial (a), residual tangential (b), and vertical (c) velocities of the OB stars.

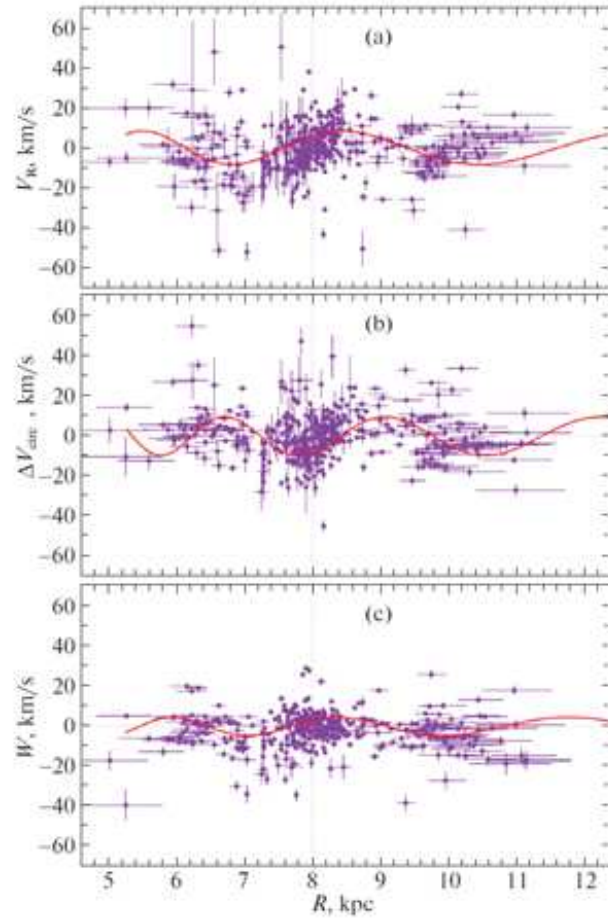


Figure 5: (Color online) Radial (a), residual tangential (b), and vertical (c) velocities of the OB stars versus Galactocentric distance; the vertical dotted line marks the Sun's position.

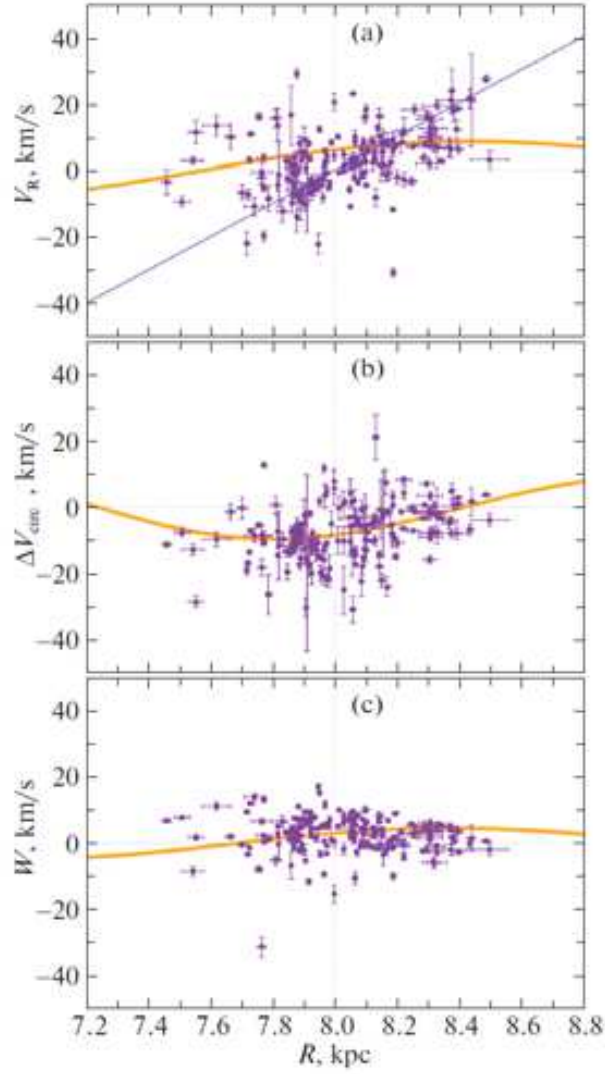


Figure 6: (Color online) Radial (a), residual tangential (b), and vertical (c) velocities of the Gould Belt OB stars versus Galactocentric distance; the vertical dotted line marks the Sun's position.

agreement in determining the wavelength of the spiral density wave, can be seen. The result obtained from the tangential velocities (Fig. 4b) should be particularly noted, because searching for the wavelength based on such velocities previously gave a considerably lower value, $\lambda_\theta = 1.9 \pm 0.6$ kpc (Bobylev and Bajkova 2017).

For checking, we calculate the pitch angle of the spiral pattern based on Eq. (9). As a result, we obtain $i_R = -14.6^\circ \pm 0.5^\circ$, $i_\theta = -10.5^\circ \pm 0.7^\circ$ and $i_W = -11.9^\circ \pm 2.4^\circ$ from the radial, residual tangential, and vertical velocities, respectively.

These results are in good agreement with the estimates of various authors made in recent years. In particular, an overview of such estimates can be found in Vallée (2017b, 2017c), where the mean values are close to $\lambda = 3.1$ kpc ($R_0 = 8.0$ kpc), $m = 4$, and $i = -13^\circ$.

Figure 5 provides the radial, residual tangential, and vertical velocities of the OB stars with the inscribed periodic dependences whose parameters were determined through a spectral analysis. Based on this figure, we determine the Sun’s radial phase in the spiral density wave measured from the center of the Carina.Sagittarius arm ($R \sim 7$ kpc). As a result, we find $(\chi_\odot)_R = -135^\circ \pm 5^\circ$, $(\chi_\odot)_\theta = -123^\circ \pm 8^\circ$ and $(\chi_\odot)_W = -132^\circ \pm 21^\circ$ from the radial, residual tangential, and vertical velocities, respectively.

On the Influence of the Gould Belt

To study the kinematic peculiarities of the Gould Belt, from our sample of OB stars we took stars with relative trigonometric parallax errors less than 15% from the solar neighborhood of radius $r = 0.6$ kpc. The produced sample contains 185 stars. The radial, residual tangential, and vertical velocities of these stars are given in Fig. 6. Just as in Fig. 5, the thick lines indicate the periodic dependences whose parameters were determined through a spectral analysis.

The thin line in Fig. 6a is given as an illustration. When analyzing our sample of OB stars with photometric distances the analogous velocity from stars close to the Sun was $dU/dR \approx 40$ km s⁻¹ kpc⁻¹ (Fig. 4 in Bobylev and Bajkova (2013)).

A crowding of points in the R range 7.8–7.9 kpc is clearly seen in all velocities of Fig. 6—in the radial, tangential and vertical ones. Analysis of their coordinates showed that these stars belong to the Scorpius–Centaurus association. The grouping manifests itself particularly clearly in the radial (Fig. 6a) velocities—the stars are aligned in a chain located at a considerable slope (approximately twice the slope of the thin line in the figure) to the horizontal axis. The interpretation here is the same as that for the Gould Belt—this is the effect of intrinsic expansion of the Scorpius–Centaurus association. Judging by the slope, the expansion coefficient of this grouping of stars is twice that for the Gould Belt.

Estimating accurate values for the expansion coefficient requires determining the position of the kinematic center; it is necessary to subtract the contributions of the Galactic differential rotation and the spiral density wave. A larger number of stars should also be involved. We are planning to perform such a work later.

Excluding ~ 150 candidates for membership in the Gould Belt has virtually no effect on the determination of the parameters of the Galactic rotation curve (see Table 1). However, the parameters of the spiral density wave being determined change in this approach. After such an exclusion we found the following parameters: the perturbation amplitudes $f_R = 4.7 \pm 0.7$ km s⁻¹, $f_\theta = 4.7 \pm 0.8$ km s⁻¹ and $f_W = 5.4 \pm 1.0$ km s⁻¹, the perturbation wavelengths $\lambda_R = 3.0 \pm 0.2$ kpc, $\lambda_\theta = 2.8 \pm 0.2$ kpc and $\lambda_W = 2.8 \pm 0.6$ kpc, and the Sun’s radial phase in the spiral density wave $(\chi_\odot)_R = -180 \pm 8^\circ$, $(\chi_\odot)_\theta = -156 \pm 14^\circ$ and

$(\chi_{\odot})_W = -120 \pm 25^\circ$, respectively. Compared to the previous case, where all OB stars were used, here the agreement in determining the wavelength λ improved, the perturbation amplitudes f_R and f_θ decreased, the agreement in the estimates of the Sun’s phase $(\chi_{\odot})_R$ and $(\chi_{\odot})_\theta$, became poorer, while for the vertical velocities, on the contrary, all parameters improved, although their random errors slightly increased.

CONCLUSIONS

We considered a sample of 554 OB stars. The line-of-sight velocities of these stars were determined through ground-based observations, while their trigonometric parallaxes and proper motions were taken from the Gaia DR2 catalogue (Brown et al. 2018).

Based on OB stars with their distances estimated from interstellar calcium lines, we made a comparison with the distance scale specified by the trigonometric parallaxes from the Gaia DR2 catalogue. As a result, our previous conclusion about the necessity of a slight (less than 20%) reduction in the calcium distance scale was corroborated by an independent method.

The parameters of the Galactic rotation curve (19) were determined from OB stars with reliable trigonometric parallax estimates (with relative parallax errors less than 30%). The derived parameters of this rotation curve were used to form the residual velocities.

The parameters of the Galactic spiral density wave were found from the series of radial, V_R , residual tangential, ΔV_{circ} , and vertical, W , velocities of OB stars by applying a periodogram analysis. OB stars with relative parallax errors less than 20% were used for such an analysis. The amplitudes of the radial, tangential, and vertical velocity perturbations are $f_R = 7.1 \pm 0.3 \text{ km s}^{-1}$, $f_\theta = 6.5 \pm 0.4 \text{ km s}^{-1}$, and $f_W = 4.8 \pm 0.8 \text{ km s}^{-1}$, respectively; the perturbation wavelengths are $\lambda_R = 3.3 \pm 0.1 \text{ kpc}$, $\lambda_\theta = 2.3 \pm 0.2 \text{ kpc}$, and $\lambda_W = 2.6 \pm 0.5 \text{ kpc}$, adopted four-armed spiral pattern ($m = 4$). The Sun’s phase in the spiral density wave is $(\chi_{\odot})_R = -135^\circ \pm 5^\circ$, $(\chi_{\odot})_\theta = -123^\circ \pm 8^\circ$, and $(\chi_{\odot})_W = -132^\circ \pm 21^\circ$.

We illustrated the influence of kinematic peculiarities of the Gould Belt stars. For this purpose, we considered stars with relative trigonometric parallax errors less than 15% from the solar neighborhood of radius $r = 0.6 \text{ kpc}$. The well-known expansion of the entire complex is clearly seen in the radial velocities. Furthermore, a fine structure manifested itself for the first time in the radial velocities of nearby OB stars. In particular, we see an intrinsic expansion of the stars belonging to the Scorpius–Centaurus association.

Excluding the Gould Belt stars hardly affects the determination of the parameters of the Galactic rotation curve. However, their exclusion has an effect when determining the parameters of the spiral density wave. After their exclusion we obtained the following estimates: the perturbation amplitudes $f_R = 4.7 \pm 0.7 \text{ km s}^{-1}$, $f_\theta = 4.7 \pm 0.8 \text{ km s}^{-1}$, and $f_W = 5.4 \pm 1.0 \text{ km s}^{-1}$, the perturbation wavelengths $\lambda_R = 3.0 \pm 0.2 \text{ kpc}$, $\lambda_\theta = 2.8 \pm 0.2 \text{ kpc}$, and $\lambda_W = 2.8 \pm 0.6 \text{ kpc}$, and the Sun’s radial phase in the spiral density wave $(\chi_{\odot})_R = -180 \pm 8^\circ$, $(\chi_{\odot})_\theta = -156 \pm 14^\circ$, and $(\chi_{\odot})_W = -120 \pm 25^\circ$, respectively.

ACKNOWLEDGMENTS

We are grateful to the referee for useful remarks that contributed to an improvement of the paper. This work was supported by the Basic Research Program P–28 of the Presidium of the Russian Academy of Sciences, the “Cosmos: Studies of Fundamental Processes and Their Interrelations” Subprogram.

REFERENCES

1. A. T. Bajkova and V. V. Bobylev, *Astron. Lett.* 38, 549 (2012).
2. C. Blaha and R. M. Humphreys, *Astrophys. J.* 98, 1598 (1989).
3. V. V. Bobylev and A. T. Bajkova, *Astron. Lett.* 37, 526 (2011).
4. V. V. Bobylev and A. T. Bajkova, *Astron. Lett.* 38, 638 (2012).
5. V. V. Bobylev and A. T. Bajkova, *Astron. Lett.* 39, 532 (2013).
6. V. V. Bobylev and A. T. Bajkova, *Mon. Not. R. Astron. Soc.* 437, 1549 (2014).
7. V. V. Bobylev and A. T. Bajkova, *Mon. Not. R. Astron. Soc.* 447, L50 (2015).
8. V. V. Bobylev and A. T. Bajkova, *Astron. Lett.* 41, 473 (2015).
9. V. V. Bobylev and A. T. Bajkova, *Astron. Lett.* 43, 159 (2017).
10. J. Bovy, *Mon. Not. R. Astron. Soc.* 468, L63 (2017).
11. A.G.A. Brown, A. Vallenari, T. Prusti, J. de Bruijne, F. Mignard, R. Drimmel, C. Babusiaux, C.A.L. Bailer-Jones, et al. (GAIA Collab.), *Astron. Astrophys.* 595, A2 (2016).
12. A.G.A. Brown, A. Vallenari, T. Prusti, J. de Bruijne, C. Babusiaux, C.A.L. Bailer-Jones, M. Biermann, D. W. Evans, et al. (GAIA Collab.), arXiv: 1804.09365 (2018).
13. T. Camarillo, M. Varun, M. Tyler, and R. Bharat, *Publ. Astron. Soc. Pacif.* 130, 4101 (2018).
14. G. A. Galazutdinov, A. Strobels, F.A. Musaev, A. Bondar, and J. Krelowski, *Publ. Astron. Soc. Pacif.* 127, 126 (2015).
15. R. de Grijs and G. Bono, *Astrophys. J. Suppl. Ser.* 232, 22 (2017).
16. J. A. S. Hunt, D. Kawata, G. Monari, R.J.J. Grand, B. Famaey, and A. Siebert, *Mon. Not. R. Astron. Soc.* 467, 21 (2017).
17. C. C. Lin and F. H. Shu, *Astrophys. J.* 140, 646 (1964).
18. L. Lindegren, J. Hernandez, A. Bombrun, S. Klioner, U. Bastian, M. Ramos-Lerate, A. de Torres, H. Steidelmuller, et al. (GAIA Collab.), arXiv: 1804.09366 (2018).
19. J. Maiz-Apellániz, *Mon. Not. R. Astron. Soc.* 121, 2737 (2001).
20. A. Megier, A. Strobels, A. Bondar, F. A. Musaev, I. Han, J. Krelowski, and G. A. Galazutdinov, *Astrophys. J.* 634, 451 (2005).
21. A. Megier, A. Strobels, G. A. Galazutdinov, and J. Krelowski, *Astron. Astrophys.* 507, 833 (2009).
22. A. M. Mel'nik and A. K. Dambis, *Mon. Not. R. Astron. Soc.* 400, 518 (2009).
23. A. M. Mel'nik and A. K. Dambis, *Mon. Not. R. Astron. Soc.* 472, 3887 (2017).
24. D. Pourbaix, A. A. Tokovinin, A. H. Batten, F. C. Fekel, W. I. Hartkopf, H. Levato, N. I. Morrell, G. Torres, and S. Udry, *Astron. Astrophys.* 424, 727 (2004).
25. T. Prusti, J.H. J. de Bruijne, A.G.A. Brown, A. Vallenari, C. Babusiaux, C.A.L. Bailer-Jones, U. Bastian, M. Biermann, et al. (GAIA Collab.), *Astron. Astrophys.* 595, A1 (2016).
26. A. S. Rastorguev, M. V. Zabolotskikh, A. K. Dambis, N. D. Utkin, V. V. Bobylev, and A. T. Bajkova, *Astrophys. Bull.* 72, 122 (2017).
27. A. G. Riess, S. Casertano, W. Yuan, L. Macri, B. Bucciarelli, M. G. Lattanzi, J.W. MacKenty, J. B. Bowers, et al., *Astrophys. J.* **861**, 126 (2018).
28. K. G. Stassun and G. Torres, *Astrophys. J.* **862**, 61 (2018).
29. The HIPPARCOS and Tycho Catalogues, ESA SP-1200 (1997).
30. J. P. Vallée, *Astrophys. Space Sci.* 362, 79 (2017a).
31. J. P. Vallée, *Astron. Rev.* 132, 113 (2017b).
32. J. P. Vallée, *New Astron. Rev.* 79, 49 (2017c).
33. V.V. Vityazev, A.S. Tsvetkov, V.V. Bobylev, and A.T. Bajkova, *Astrophysics* 60, 462 (2017).
34. M. V. Zabolotskikh, A. S. Rastorguev, and A. K. Dambis, *Astron. Lett.* 28, 454 (2002).
35. J. C. Zinn, M. H. Pinsonneault, D. Huber, and D. Stello, arXiv: 1805.02650 (2018).